

CMOD5.N: A C-band geophysical model function for equivalent neutral wind

Hans Hersbach

Research Department

April 2008

*This paper has not been published and should be regarded as an Internal Report from ECMWF.
Permission to quote from it should be obtained from the ECMWF.*



European Centre for Medium-Range Weather Forecasts
Europäisches Zentrum für mittelfristige Wettervorhersage
Centre européen pour les prévisions météorologiques à moyen terme

Series: ECMWF Technical Memoranda

A full list of ECMWF Publications can be found on our web site under:

<http://www.ecmwf.int/publications/>

Contact: library@ecmwf.int

©Copyright 2008

European Centre for Medium-Range Weather Forecasts
Shinfield Park, Reading, RG2 9AX, England

Literary and scientific copyrights belong to ECMWF and are reserved in all countries. This publication is not to be reprinted or translated in whole or in part without the written permission of the Director. Appropriate non-commercial use will normally be granted under the condition that reference is made to ECMWF.

The information within this publication is given in good faith and considered to be true, but ECMWF accepts no liability for error, omission and for loss or damage arising from its use.

Abstract

This document describes the evaluation of a C-band geophysical model function. This model function, called CMOD5.N, is to provide an empirical relation between C-band backscatter as sensed by the space-born ERS-2 and ASCAT scatterometers, and equivalent neutral ocean vector wind at 10-metre height (neutral surface wind) as function of (scatterometer) incidence angle.

CMOD5.N embodies a refit of CMOD5, a C-band model function which was previously derived to obtain non-neutral surface wind, in such a way that its 28 tuneable coefficients lead, for given backscatter observation, to an enhancement of 0.7ms^{-1} in wind speed. The value of 0.7ms^{-1} is chosen to be independent on wind speed and incidence angle, and incorporates the average difference between neutral and non-neutral wind ($\sim 0.2\text{ms}^{-1}$) and for a known bias of CMOD5 ($\sim 0.5\text{ms}^{-1}$) when compared to buoy wind data.

The quality of the CMOD5.N fit is tested for the AMI scatterometer on ERS-2 and ASCAT instrument on METOP-A for July 2007 and January 2008. From this it is found that winds inverted with CMOD5.N are on average 0.69ms^{-1} stronger than winds determined from CMOD5. As function of wind speed and incidence angle, fluctuations are well within 0.05ms^{-1} . Differences in wind direction are small.

ASCAT and ERS-2 wind speed obtained from CMOD5.N compares on average well with operational neutral wind from the European Centre for Medium-Range Weather Forecasts (ECMWF). In comparison with non-neutral wind, local, seasonally dependent biases between scatterometer and ECMWF model are reduced. Besides effects introduced by orography and ocean currents, a residual stability-dependent bias between scatterometer and neutral wind remains, which is likely connected to a previously reported non-optimality in the ECMWF boundary layer formalism by Brown *et al.* in 2006.

The work presented in this document is funded by ESRIN (Project Ref. 18212/04/I-OL).

1 Introduction

Space-born scatterometer data provide accurate information on speed and direction of surface wind over the global oceans. Since the launch of the ERS-1 satellite in July 1991, global coverage of scatterometer data has been available without interruption. Applications vary from near-real time assimilation into numerical weather prediction models (NWP), the forcing of ocean models, to climate studies accessing the now 17-year data record.

At the European Centre for Medium-Range Weather Forecasts (ECMWF) scatterometer winds have been assimilated in the operational integrated forecast and assimilation system (IFS) from 30 January 1996 onwards. The four-dimensional variational assimilation system at ECMWF allows for a dynamically consistent use of observations. In this way, information of scatterometer surface winds is propagated to the entire troposphere (Isaksen and Janssen, 2004). Currently (April 2008) data is used from the AMI scatterometer on-board the European Remote sensing Satellites ERS-2 (from June 1996 onwards), the SeaWinds instrument on-board QuikSCAT (from January 2002 onwards), and from the ASCAT instrument on the MetOp-A platform (from June 2007 onwards). Thanks to the different timing of ascending nodes of these three satellites, most areas on the globe are covered within a six-hour period. Morning and afternoon are captured by QuikSCAT, while noon and midnight are served by ASCAT and ERS-2. An example is given in Figure 1, which shows the observation of an intense low near the British Isles by ASCAT and ERS-2 around 00 UTC 9 December 2007.

A scatterometer is a microwave radar that emits pulses at well-defined frequency and polarization to the Earth surface. A backscatter is recorded, from which information on the sensed surface can be obtained. In polar regions characteristics and age of sea ice can be determined, over land information on soil moisture can be extracted, while over open water an estimate of the surface vector wind can be obtained. It is this latter application that has been known longest. The main physical process is based on Bragg scattering where backscatter is related to the intensity of surface water waves with wavelengths that are comparable to that of the emitted pulse.

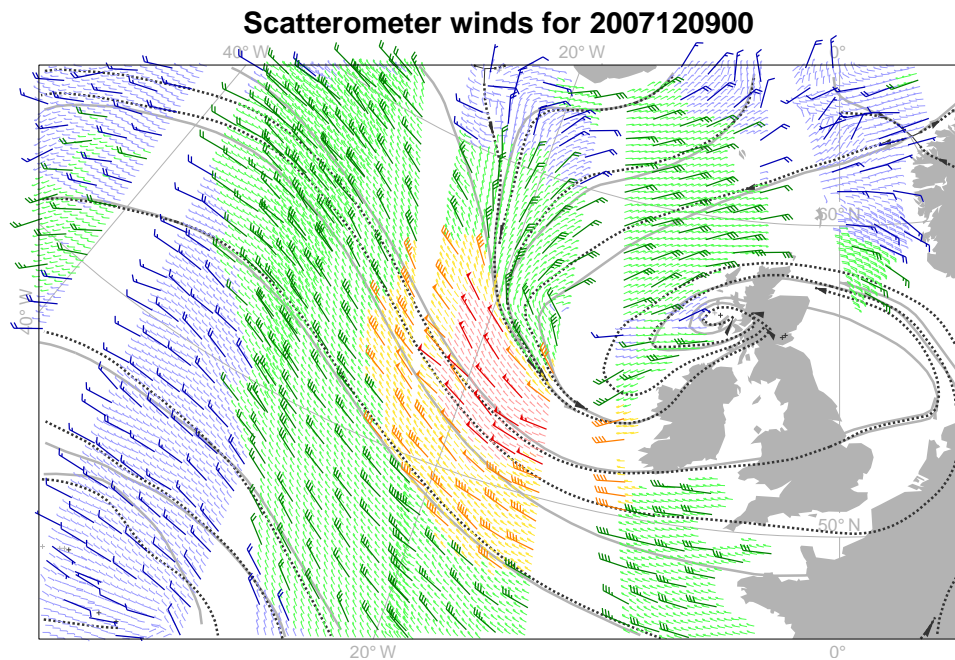


Figure 1: Scatterometer winds from ERS-2 and ASCAT as assimilated at ECMWF for the 12-hour assimilation cycle of 00 UTC 9 December 2007. The two tracks around 40W and the track parallel to 10W concern ASCAT data; the three tracks around 45W, 20W and 0W originate from ERS-2. Large barbs indicate actively assimilated winds and small barbs indicate rejected (mostly thinned) winds. Colors indicate speed ranges (blue less than 10m s^{-1} , green $10\text{-}20\text{m s}^{-1}$, orange $20\text{-}25\text{m s}^{-1}$, and red exceeding 25m s^{-1}). Black and grey lines represent streamlines for the ECMWF analysis and first-guess surface winds.

By choice of the scatterometer wavelength in the centimetre range, the strength of capillary surface waves is sensed. These in turn, are determined by the local surface stress, or in effect, the local surface wind condition. Since backscatter response also depends on the relative angle between the incident pulse and capillary wave direction, information on wind direction can be extracted as well.

Although the physical mechanism is in principle known, for practical applications the relation between wind and backscatter is provided by an empirical geophysical model function. Such a model function is the result of a large collocation study between observed (aircraft and/or spaceborn) scatterometer backscatter with in situ buoy data and/or NWP model data. Backscatter should correlate most closely with surface stress. Since this quantity cannot be obtained accurately from in situ observations, in practice readily available winds at a standard height of 10m are used, instead. Typical variations in the relation between stress and wind mainly depend on atmospheric stability and ocean-wave sea state.

For the C-band (5.3 GHz) AMI scatterometers on-board ERS-1 and ERS-2, and ASCAT on-board Metop-A, a branch of model functions with common name CMOD (C-band model) have been developed in the past. These are all based on collocation studies with observed and/or modelled wind at 10 metre height.

For the Ku-band frequency (13.4 GHz) at which the scatterometer on-board QuikSCAT operates, as well as the SeaWinds and NSCAT instruments on-board the past ADEOS-II respectively ADEOS-I platforms, geophysical model functions have been traditionally trained on neutral equivalent winds (Wentz and Smith 1999, Freilich and Dunbar 1999, Ebuchi *et al.* 2002; for an overview see Chelton and Freilich 2005). Such winds (from now on simply denoted by neutral) represent the wind at 10-metre height for given surface stress in case the marine boundary layer were neutrally stratified. They can be estimated from real winds (to be called non-

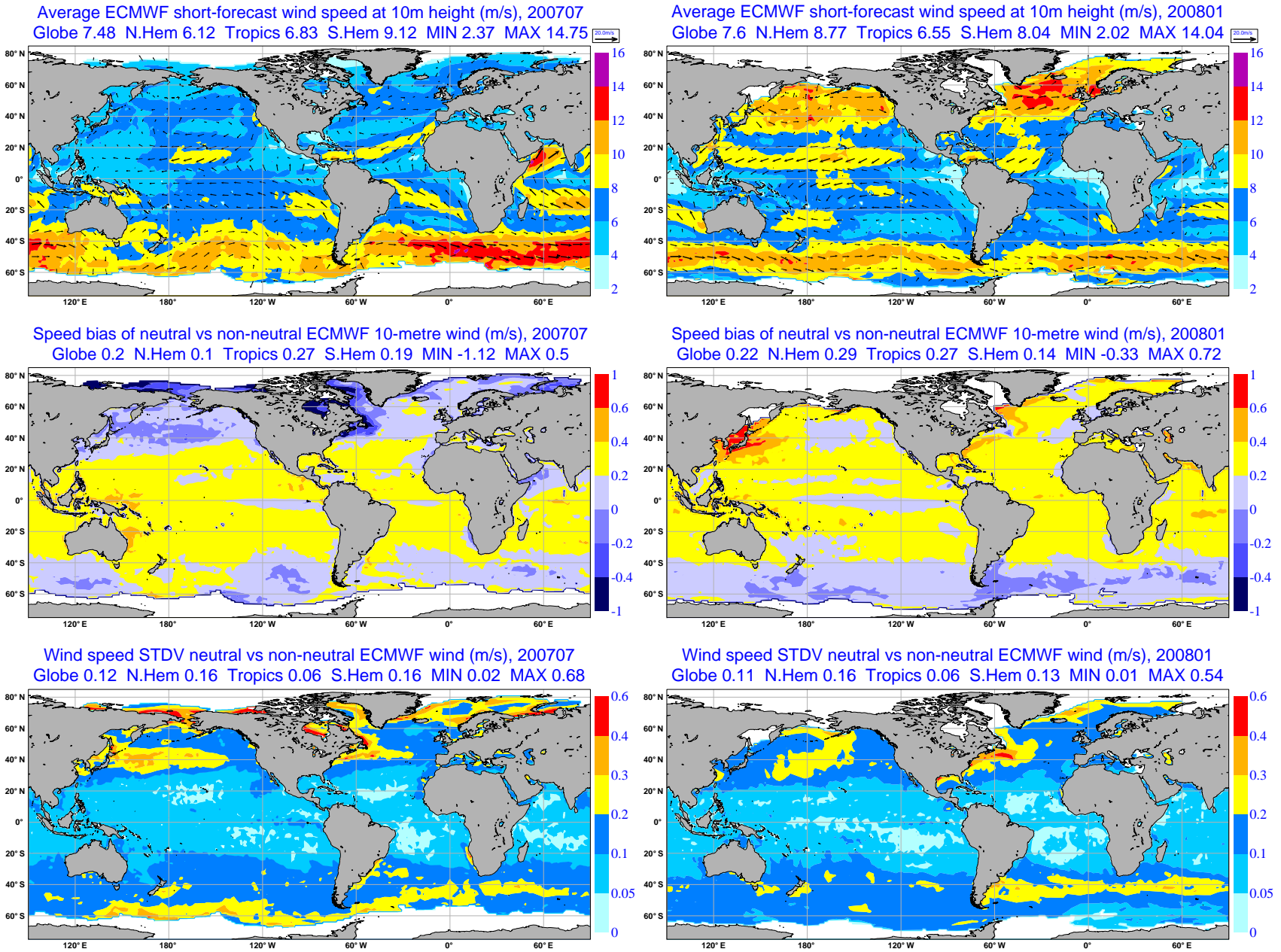


Figure 2: Average ocean wind speed (colors) and ocean vector wind (arrows) at 10m height (top panels), and average difference (middle panels) and standard deviation (lower panels) from equivalent neutral wind speed, for the operational ECMWF short-range forecast at ASCAT location during July 2007 (left panels) and January 2008 (right panels).

neutral from now on) at 10-metre or buoy observation height by transformation of such winds to surface stress by taking account of additional information on atmospheric stability, and subsequently transforming back to 10-metre wind by the neglect of these stability effects. Although the intermediate values for surface stress may depend sensitively on the details of the boundary layer model under consideration, the final differences between neutral and non-neutral wind appear more robust. Rationale behind this is that the model-dependencies in the transformation from (non-neutral) wind to stress are largely undone when transforming back from stress to (neutral) wind. Therefore, by using neutral wind, the case dependent effect of stability can be incorporated without having to know actual values for stress.

On average, the marine boundary layer is weakly unstable, and the global average neutral wind appears $\sim 0.2\text{m s}^{-1}$ stronger than the non-neutral wind. Stability is for a large extent determined by the difference between surface air temperature and sea-surface temperature (SST). Locally, average neutral effects correlate with the typical weather regime in relation to (the slower) SST component, while fluctuations correlate more with variations in the (faster) meteorological component. An example of this is presented in Figure 2, where statistics of stability effects, as calculated in the IFS system (IFS documentation, 2004), are summarized for short-range ECMWF model wind for July 2007 and January 2008¹. In Northern Hemispheric summer (left-hand middle panel) a stable boundary layer exists in the Arctic region, the North-American Great lakes and the area east of Newfoundland. It is induced by warm off-land and or southerly maritime wind over cooler ocean water. In these areas neutral winds can be lower than non-neutral winds by 0.5m s^{-1} . The right-hand middle panel shows a similar, though less intense effect off Patagonia over the summer Southern Hemisphere. Northern Hemispheric winter clearly shows the signature of an enhanced SST in the Gulf stream and the Kuroshio Extension. In both hemispheres winds are more unstable in winter and less unstable during summer, although the difference is largest on the Northern Hemisphere. The lower panels of Figure 2 show that locally, fluctuations around the mean can be larger than the average difference. This is e.g., the case in the storm tracks, where the movement of weather systems alternates the presence of stable and unstable conditions. On the other hand, fluctuations are small in the regions of steady trade winds.

Various studies have confirmed the response of scatterometer data to surface stress (see, e.g., Chelton *et al.* 2004 for a detailed description for QuikSCAT data). Hence, as a first step, it is desirable to derive a C-band geophysical model function for neutral wind rather than non-neutral. This will be the objective in this study. This model function, which is called CMOD5.N is based on the CMOD5 model function, by a refit of 28 tunable coefficients.

In Section 2 the most popular CMOD models are briefly reviewed, and the requirement for CMOD5.N will be formulated. The refit of the 28 coefficients is described in Section 3. The quality of the fit for scatterometer data from ERS-2 and ASCAT will be the subject of Section 4. In Section 5, a detailed comparison is made between CMOD5.N scatterometer winds and both neutral and non-neutral ECMWF winds. The memorandum ends with some concluding remarks.

2 The C-band CMOD family

The development of the CMOD family was initialised by the requirement of a geophysical model function for the C-band AMI scatterometer on-board ERS-1 that was launched by the European Space Agency (ESA). The AMI instrument (Attema, 1986, Francis, 1991) obtains backscatter measurements from three antennas (fore, mid, aft), illuminating a swath of 500 km, in which 19 nodes, or wave-vector cells (WVC), define a 25 km product. From these backscatter triplets, two similarly likely, near anti-parallel solutions can be retrieved.

¹only ECMWF winds were used that collocate with ASCAT observations and where sea-ice fraction was below 10% and SST above 273.15 K. This restriction is not essential for the discussion.

All CMOD models provide an empirical functional relation in which the dependency of normalized backscatter σ_0 on wind speed v , wind direction χ , and incidence angle θ is described as:

$$\sigma_0 = \text{CMOD}(\mathbf{c}, v, \phi, \theta) = \text{B0}(\mathbf{c}_0, v, \theta) [1 + \text{B1}(\mathbf{c}_1, v, \theta) \cos(\phi) + \text{B2}(\mathbf{c}_2, v, \theta) \cos(2\phi)]^p. \quad (1)$$

Here $\phi = \chi - \alpha$ is the angle between wind direction and scatterometer azimuth look angle (both measured from the North), coefficients \mathbf{c} (which are subsets from a larger set \mathbf{c}) shape the terms B_i , and p is a parameter. The dependency on wind direction is described by only two harmonics. The dominant term B0 sets the speed scale for a given measurement. The upwind-crosswind asymmetry B2 allows for the determination of wind direction, while B1 attributes to resolve a remaining 180-degree ambiguity in wind direction.

The first model, CMOD2 (Long 1985) was a pre-launch model function that was based on airborne data. After the launch of ERS-1 it soon appeared inadequate, and a replacement, called CMOD4 was developed by Stoffelen and Anderson (1997) using actual data from ERS-1. Besides a reformulation, the innovative part was the introduction of $p = 1.6$, rather than unity. It effectively avoids the need in (1) for higher harmonics B3 , B4 , etc. After a selection exercise between various model function candidates (Offiler, 1994) ESA decided to base the operational ERS wind product (called UWI) on this model function, and it still is for ERS-2 today.

Although the CMOD4-based wind product meets ESA's original instrument requirements, it could be improved in several ways. Besides a negative speed bias that largely depends on incidence angle and wind speed (induced by a non-optimal description for B0), there was independent evidence from field experiments (Carswell *et al.* 1999, Donnelly *et al.* 1999, Esteban *et al.* 2006) for inadequacies in the formulation of B1 and B2 as well. Most of these issues were resolved by the development of CMOD5 (Hersbach *et al.* 2007). CMOD5 gives rise to a more uniform performance across the AMI swath. Improvements are especially obtained for extreme cases, and CMOD5 extends the dynamical range for C-band scatterometer data from 24 m s^{-1} to 35 m s^{-1} .

The CMOD5 model function had been derived on the basis of a collocation study between ERS-2 AMI triplets and ECMWF short-range forecast winds. Here it was assumed that these ECMWF winds represent an unbiased reference for surface winds over the global oceans. However, being a function of time (i.e., depending on the ECMWF model version), biases in these fields are known to exist (for a comparison with QuikSCAT winds see e.g., Chelton and Freilich, 2005). A triple collocation with buoys (which are generally believed to provide unbiased estimates of the ground truth) in the North Atlantic and North Pacific for a one-year period (August 1998 to July 1999) showed that both CMOD5 and ECMWF FGAT winds were biased low by about 0.35 m s^{-1} . This bias was found to be uniform, i.e., independent on wind speed itself (see Fig. 13 of Hersbach *et al.* 2007). A similar study by Abdalla and Hersbach (2007), in which the collocation period was extended to two three year periods, one for ERS-1 and one period for ERS-2, displayed a reasonably flat bias of -0.55 m s^{-1} for ERS-2. For ERS-1 a wind-speed dependent bias of on average -0.24 m s^{-1} emerged. The difference of 0.31 m s^{-1} indicates a difference in calibration between ERS-1 and ERS-2. An analysis performed by Portabella and Stoffelen (2007) for ERS-2 data, which included the TAO buoy network in the tropics, indicated a negative bias for CMOD5 of around 0.50 m s^{-1} .

Although all analyses presented above confirm that CMOD5 is biased low, they disagree in the exact amount. For ERS-2 estimates vary between -0.35 m s^{-1} and -0.55 m s^{-1} . A value of $-0.45 \pm 0.10 \text{ m s}^{-1}$ seems reasonable. It appeared that such a difference can be incorporated in the original CMOD5 formulation by a refit of its 28 coefficients. As a result, winds inverted by this retuned model function, called CMOD5.4, appear 0.48 m s^{-1} stronger than winds based on CMOD5. Details may be found in Abdalla and Hersbach (2007). CMOD5.4 has been used in the operational assimilation system at ECMWF since June 2007 for both ERS-2 and ASCAT (e.g., for the case displayed in Figure 1).

For winds in the near-real time level 2 ASCAT product disseminated by the data provider EUMETSAT (European Organisation for the Exploitation of Meteorological Satellites), a slightly different approach is followed.

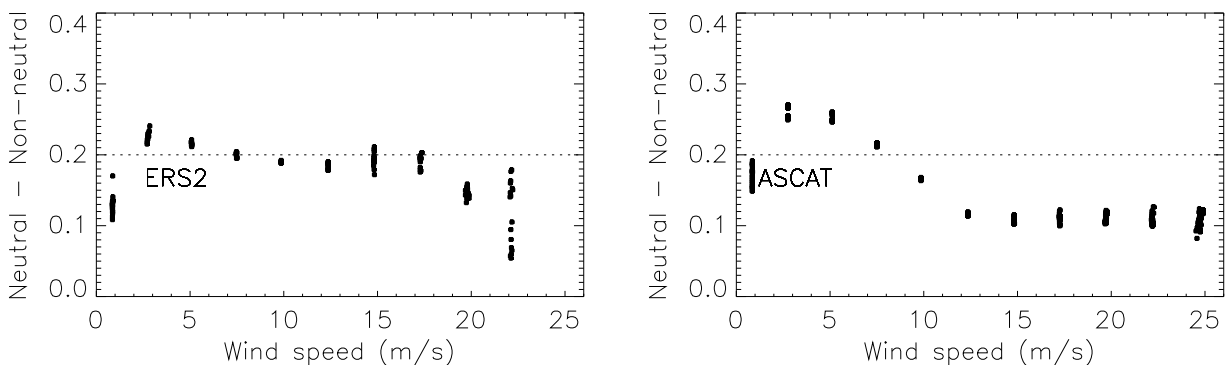


Figure 3: Average relation between ECMWF neutral and non-neutral wind speed (m s^{-1}) at ERS-2 location (left-hand panel), and ASCAT location (right-hand panel), summed over July 2007 and January 2008. Data points represent wave-vector cell wise (19 for ERS-2; 42 for ASCAT) averages in speed bins of 2.5 m s^{-1} for which at least 100 data points were available. Average difference is 0.20 m s^{-1} for both ERS-2 and ASCAT.

The ASCAT instrument (Figa-Saldaña *et al.* 2002) is of similar design to AMI, the main differences being a different range of incidence angles, and two sets of antennas providing two swathes. In each swath 21 WVC's form a 25km product, i.e. 42 in total. The transformation of backscatter to wind is delivered by the Koninklijk Nederlands Meteorologisch Instituut (KNMI) within the EUMETSAT Ocean and Sea Ice SAF framework. Here, winds are based on CMOD5, however after inversion 0.5 m s^{-1} is added to wind speed. This model function is called CMOD5.5.

To summarize, there is a pre-launch model function CMOD2, an operational ERS-2 model function CMOD4, and an improved model function CMOD5, which has two very similar derivatives CMOD5.4 and CMOD5.5 that both correct for a bias of $\sim -0.5 \text{ m s}^{-1}$ in CMOD5. All are tuned for non-neutral wind.

As discussed in the introduction, the global average neutral wind is around 0.2 m s^{-1} stronger than the global average non-neutral wind. To investigate this difference when limited to cases covered by ERS-2 and ASCAT, and its dependency on the value of wind speed as well, the ECMWF winds are collocated with ERS-2 and ASCAT data for the periods of July 2007 and January 2008 (i.e., as in Figure 2). ECMWF winds are bilinearly interpolated to scatterometer observation location, and in time the closest field (resolution of 3 hours) is used. Only data is regarded where ECMWF fields for sea ice fraction and SST have respectively local values below 10% and above 273.15 K. Statistics between ECMWF neutral and non-neutral winds are determined for different speed bins (2.5 m s^{-1} each), and for each scatterometer wave vector cell. Average differences are presented in Figure 3. From this it is seen that the dependency on wind speed is low for the locations sensed by ERS-2, while for ASCAT the difference between neutral and non-neutral wind speed is lower for winds above 10 m s^{-1} . The variation at strong wind speed, where statistics is lower, depends on the details of the sampling of the underlying conditions. Besides, the average dependency of neutral effects on wind speed is probably within the uncertainty of similar dependencies of the CMOD5 bias. Therefore, it is proposed that an unbiased CMOD5.N model function for neutral winds should provide winds that are 0.7 m s^{-1} stronger than obtained by CMOD5, independent on wind speed (and of course incidence angle). This amount is the sum of the bias in CMOD5 (0.5 m s^{-1}) and stability correction (0.2 m s^{-1}). Rather than adding 0.7 m s^{-1} to wind speed after inversion (i.e., CMOD5.5 style), the 28 coefficients will be retuned (i.e., CMOD5.4 approach).

3 Determination of the coefficients for CMOD5.N

The objective is to retune the 28 CMOD5 coefficients such that an inversion scheme will deliver winds that are 0.7 m s^{-1} stronger. This can be achieved by demanding that for given wind speed CMOD5 should give exactly the same backscatter as CMOD5.N for a wind that is 0.7 m s^{-1} stronger. Given formulation (1) this leads to the following set of conditions:

$$\begin{aligned} \text{B0}(\mathbf{c}'_{01-13}, v + 0.7 \text{ m s}^{-1}, \theta) &= \text{B0}(\mathbf{c}_{01-13}, v, \theta) \\ \text{B1}(\mathbf{c}'_{14-18}, v + 0.7 \text{ m s}^{-1}, \theta) &= \text{B1}(\mathbf{c}_{14-18}, v, \theta) \\ \text{B2}(\mathbf{c}'_{19-28}, v + 0.7 \text{ m s}^{-1}, \theta) &= \text{B2}(\mathbf{c}_{19-28}, v, \theta) \end{aligned} \quad (2)$$

Here \mathbf{c} and \mathbf{c}' are respectively the original and retuned set of coefficients, and the indices show the range of coefficients that define each term. Values of B0, B1, and B2 as function of wind speed and incidence angle are displayed in the left panels of Figures 4-6. Details on the CMOD5 formulation may be found in Hersbach *et al.* (2007). Of course, relation (2) cannot be satisfied for all combinations within the in practice encountered range of wind speed v and incidence angle θ . For each term, therefore, a cost function J_i is to be defined, and a fit involving the relevant part of \mathbf{c}' has to be performed:

$$J_i = \langle \delta_i^2(v, \theta) \rangle, \quad i = 0, 1, 2 \quad (3)$$

Here δ_i expresses a departure from the ideal state, and $\langle \cdot \rangle$ denotes some weighted average over a certain domain in wind speed and incidence angle.

It would be tempting to define δ_i just as the amount at which (2) is violated:

$$\delta_i = \text{Bi}(\mathbf{c}', v + 0.7 \text{ m s}^{-1}, \theta) - \text{Bi}(\mathbf{c}, v, \theta) \quad (4)$$

For B0, though, one should realize that its dynamical range is over a few orders of magnitude. In decibel units ($\text{dB} \equiv 10 \log \sigma_0$), e.g., B0 ranges from -30 dB for light wind at $\theta = 55$ degrees to 0 dB for hurricane wind speed at $\theta = 20$ degrees. Typical observation error in backscatter is a few percent, or around 0.2 dB . Therefore, a certain misfit in σ_0 might, compared to observation error, be insignificant for one case, but huge for another case. An alternative would be to define departures δ_i in decibel units. Although now a more balanced weight is given in terms of observation error, one should realize how the wind inversion scheme would project a normalized deviation from (2) back to a shift in wind speed. As can be seen from the left panel of Figure 4, at low wind speed, a small shift in wind speed corresponds to a larger shift in dB than at strong wind speed. Therefore, given a similar misfit in dB, the effect on wind speed will be small for light and large for strong winds. Since it is the homogeneity in the inverted wind product that ultimately matters it makes more sense to choose δ_i equal to the shift in wind speed b that is required to mend relation 2:

$$\delta_i = b(v, \theta) - 0.7 \text{ m s}^{-1}, \quad \text{for } b \text{ such that } \text{Bi}(\mathbf{c}', v + b, \theta) = \text{Bi}(\mathbf{c}, v, \theta). \quad (5)$$

In this way, deviations from (2) are automatically transformed appropriately to wind speed space. For B1 and B2 the exact choice for departure δ_i is less critical, since wind speed dependency is mainly determined by B0. For convenience, though, (5) can be used for these terms as well.

Cost function (3) is minimized over a domain in wind speed from 1 m s^{-1} to 50 m s^{-1} (in 1 m s^{-1} steps), and from 17 to 66 degrees (1 degree steps) for incidence angle. This covers both the range of ERS-2 and ASCAT (horizontal lines in Figures 4-6). For winds of 25 m s^{-1} and stronger, the weight is reduced by a factor 4. In this way the behaviour at extreme wind acts as a constraint without dominating the total cost. At local extrema of Bi , i.e., where $\partial \text{Bi} / \partial v = 0$, a solution for b is less sharply defined or it may not even exist. For this reason,

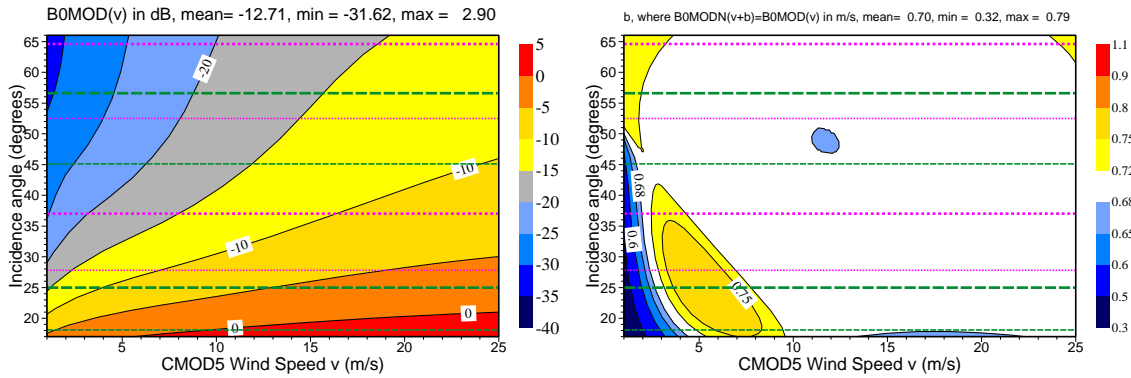


Figure 4: B_0 for CMOD5 as function of wind speed v and incidence angle θ in dB (left), and the wind speed shift b (in m s^{-1}) for which $B_0(v+b, \theta)$ based on CMOD5.N coefficients equals $B_0(v, \theta)$ using original CMOD5 coefficients (right). Green dashed horizontal lines mark the incidence-angle range for ERS-2 (thin for mid, fat for fore/aft antenna); purple dotted horizontal lines show the corresponding range for ASCAT.

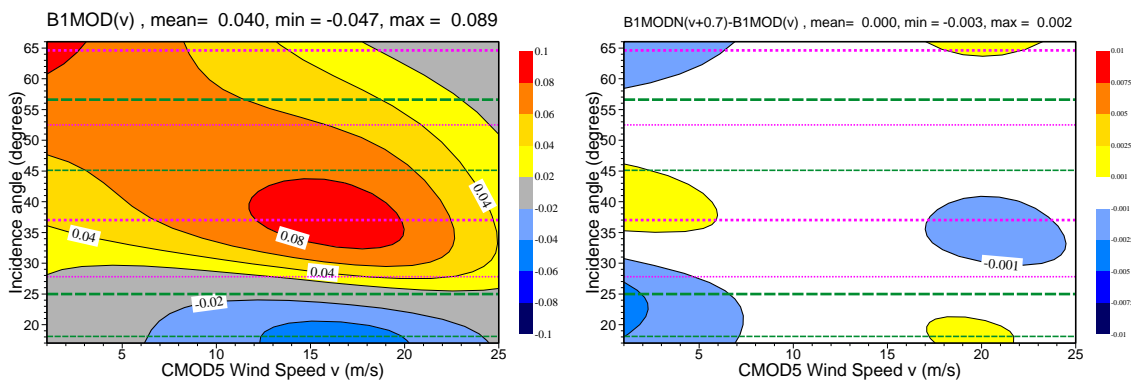


Figure 5: The same as Figure 4 but now for B_1 in natural units (left), and the difference between fit (2) (right).

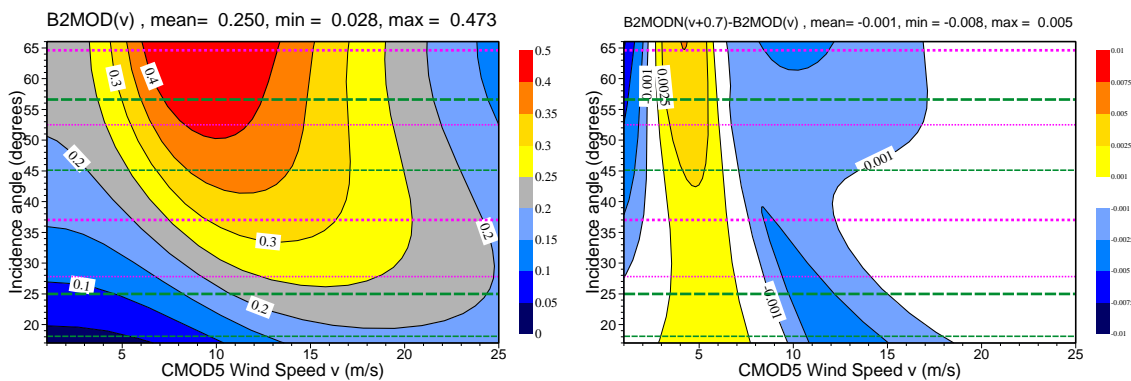


Figure 6: The same as Figure 5 but now for B_2 ,

	CMOD5	CMOD5.N		CMOD5	CMOD5.N
c_1	-0.6880	-0.6878	c_{15}	0.0070	0.0066
c_2	-0.7930	-0.7957	c_{16}	0.3300	0.3222
c_3	0.3380	0.3380	c_{17}	0.0120	0.0120
c_4	-0.1730	-0.1728	c_{18}	22.000	22.700
c_5	0.0000	0.0000	c_{19}	1.9500	2.0813
c_6	0.0040	0.0040	c_{20}	3.0000	3.0000
c_7	0.1110	0.1103	c_{21}	8.3900	8.3659
c_8	0.0162	0.0159	c_{22}	-3.4400	-3.3428
c_9	6.3400	6.7329	c_{23}	1.3600	1.3236
c_{10}	2.5700	2.7713	c_{24}	5.3500	6.2437
c_{11}	-2.1800	-2.2885	c_{25}	1.9900	2.3893
c_{12}	0.4000	0.4971	c_{26}	0.2900	0.3249
c_{13}	-0.6000	-0.7250	c_{27}	3.8000	4.1590
c_{14}	0.0450	0.0450	c_{28}	1.5300	1.6930

Table 1: CMOD5 and CMOD5.N coefficients

points that are within 1 m s^{-1} of an extremum are excluded. For B0 this only occurs for extreme wind speed at low incidence angle, while for B1 and B2 extrema are located at more moderate wind speed.

A minimization package as provided by Numerical Recipes (Press *et al.* 1997) that is based on the Powell conjugate method, was used. It does not require derivative information. Line searches needed within this method, as well as the line search required for the determination of b in (5) are based on a Brent method. Some coefficients are either fixed or recalculated by hand in case this makes sense from the start. In total 11 coefficients are fitted for B0, 4 for B1 and 9 for B2.

The resulting set \mathbf{c}' is displayed in Table 1. The normalized cost function (3) before (i.e. using $\mathbf{c}' = \mathbf{c}$) and after minimization is displayed in the second column in Table 2. Cost (3), but now evaluated for choice (4) is displayed in the third column. Here, (4) is in decibel units for B0, and situations close to extrema are now included. Note that it only serves a diagnostic purpose, i.e., this cost was not used in the minimization. The fourth column in Table 2 shows the maximum effect on backscatter over all wind speeds, wind directions and incidence angles, that can be induced by the misfit in each term. It is based on the first order Taylor expansion:

$$\delta(\text{dB}) = \delta(\text{dB0}) + A \cos(\phi) \delta(\text{B1}) + A \cos(2\phi) \delta(\text{B2}) + \dots, \quad (6)$$

where the misfit $\delta(\text{dB})$ in σ_0 and $\delta(\text{dB0})$ in B0 are in decibel, and

$$A = 16 \log(e) / (1 + \text{B1} \cos \phi + \text{B2} \cos 2\phi). \quad (7)$$

The scaling factors that transform a deviation from B1 and B2 (in natural units) to an effect on backscatter (in dB), depend on relative wind direction. For given wind speed and incidence angle, maximum values appear to range from 5 to 7 for B1 and from 7 to 13 for B2.

For B0, the result of the minimization is satisfactory. The weighted average deviation is 0.046 m s^{-1} . A detailed view of b (see right panel of Figure 4) shows that for a large part in the (v, θ) plane CMOD5.N is expected to give winds that are within 0.02 m s^{-1} from 0.7 m s^{-1} . Only for light winds at lower incidence angle deviations are larger, and it is this region that contributes most heavily to the cost. For ASCAT and ERS-2, wind speed is mainly determined by the fore and aft beam. Since incidence angles for these beams start at respectively 37 and 25 degrees, deviations in wind retrieval are (especially for ASCAT) expected to be within a few cm s^{-1} . Deviation in backscatter (third column in Table 2) is on average 0.01dB. This is on the discretization level of

B	Wind speed (m s^{-1})		Backscatter (dB for B0)		Max difference (dB)	
	CMOD5	CMOD5.N	CMOD5	CMOD5.N	CMOD5	CMOD5.N
0	0.700	0.046	0.567	0.010	2.57	0.85
1	0.700	0.343	0.014	0.005	0.04	0.02
2	0.700	0.164	0.114	0.015	0.48	0.07

Table 2: Square root of cost J_i in wind-speed space (in m s^{-1}) and backscatter space (in dB) averaged over wind speed from 1 to 50 m s^{-1} (steps of 1 m s^{-1}) and incidence angle from 17 to 60 degrees (steps of 1 degrees), at respectively the start (CMOD5 coefficients) and the end (CMOD5.N coefficients) of the minimization

σ_0 reported by the data provider (i.e., 0.01dB), and, therefore, very small. For all winds above 15 m s^{-1} the deviation is below 0.01dB. Largest deviation (0.85dB) occurs for low wind speed at low incidence angle. Since here sensitivity of backscatter on wind speed is maximal, its effect on inverted wind speed will be limited. In fact, this was the reason for the choice (5), rather than (4).

For B1 and B2 the reduction in cost is less than for B0. One reason for this is that these terms are relatively slowly varying functions of wind speed. A small error in σ_0 is transformed back to a large shift in wind speed. As mentioned above, though, these terms do not set the wind speed scale. The (diagnostic) reduction in cost when calculated in terms of deviations (4) is larger, especially for B2 (third column of Table 2). Lower panels of Figures 5, 6 show that the differences from relation (3) are tiny and the maximum effect on backscatter is very small (column 4 of Table 2). Note that for B1, usage of CMOD5 coefficients would only give a maximum error of 0.04dB to start with.

4 Validation of the CMOD5.N fit

The optimization of the CMOD5.N coefficients as performed in the previous section does not involve any wind inversion. Rationale is that, as long as the cost function (3) is used in combination with the departures (5), any inversion scheme should retrieve winds that are on average 0.7 m s^{-1} stronger compared to CMOD5. In this section this will be verified for the wind products from ERS-2 and ASCAT as inverted and assimilated at ECMWF. Here, such inversions are based on the PRESCAT algorithm (Stoffelen and Anderson, 1997). It uses a pre-calculated look-up table of CMOD backscatter as function of wind speed (1 to 60 m s^{-1} in bins of 0.5 m s^{-1}), relative wind direction (bins of 5 degree), and incidence angle (15 to 69 degrees in 1 degree bins). As a result, the inverted wind product is discretized into steps of 0.5 m s^{-1} in speed and 5 degrees in direction. Winds below 1 m s^{-1} are rejected. Two almost equally likely wind solutions are obtained which are usually nearly anti parallel. The analysis given below will only involve that solution that matches the ECMWF wind field best. Prior to wind inversion there is the possibility to correct backscatter, and after inversion wind speed can be corrected as well. These can compensate for inconsistencies in the calibration of backscatter by respectively the data provider and for residual errors in the applied CMOD function. For ERS-2 such corrections are not used, for ASCAT they are.

So far, the full calibration of the ASCAT backscatter product as provided by EUMETSAT has not been finalized. Comparison of measured backscatter with backscatter obtained from collocated ECMWF wind subjected to CMOD5.4 (known as ocean calibration, see Stoffelen 1999) reveals inaccuracies in calibration by up to -1 dB , which, in addition appear a function of WVC and antenna. The details of these corrections has changed each time EUMETSAT has updated calibration. The left panels of Figure 7 displays the sets of corrections used at ECMWF during June 2007 and January 2008. These are similar to corrections used at KNMI (and based on CMOD5.5) for the production of the level-2 ASCAT product (Verspeek *et al.* 2007). After wind inversion, comparison with ECMWF wind still shows some residual speed biases. They mainly occur at high wind speed

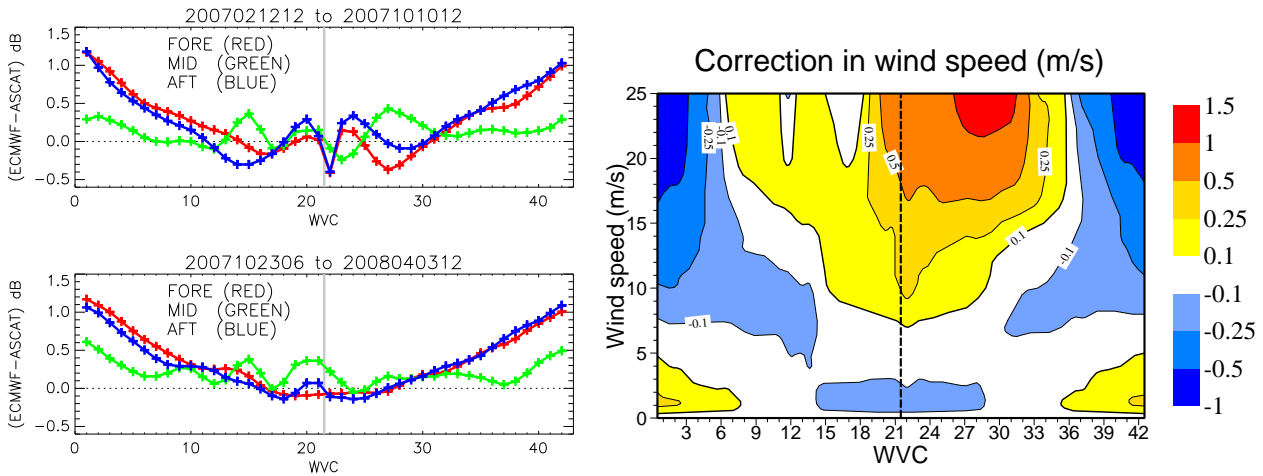


Figure 7: Bias correction (in dB) applied to ASCAT backscatter before wind inversion (left) as function of WVC and antenna (fore in red, mid in green, aft in blue) as used at ECMWF for indicated period, and additional correction in wind speed ($m s^{-1}$) after inversion (right) as function of WVC and wind speed. Minimum and maximum values in speed correction are respectively $-0.81 m s^{-1}$ and $1.20 m s^{-1}$.

for some wave vector cells. At the moment it is not clear whether these are connected to residual effects from incomplete calibration, or indicate inaccuracies in CMOD5(.4). The corrections as used at ECMWF since the operational implementation of ASCAT on 12 June 2007 is shown in the right-hand panel of Figure 7.

ERS-2 and ASCAT winds based on CMOD5 and CMOD5.N are each inverted for July 2007 and January 2008. From this it appears that for both ERS-2 and ASCAT, CMOD5.N winds are on average $0.69 m s^{-1}$ stronger than CMOD5. Scatter is low ($0.32 m s^{-1}$ for both instruments) and is mainly induced by the discretization into $0.5 m s^{-1}$ bins for each product. When stratified with respect to wind speed and scatterometer WVC, results are consistent. This is summarized in Figure 8, where each point represents the mean \mathbf{a} of the following conditional averages:

$$\mathbf{a} = \frac{1}{2}(\mathbf{a}_x + \mathbf{a}_y), \quad \text{where} \quad \begin{cases} \mathbf{a}_x \equiv (\langle x \rangle, \langle y - x \rangle) & \text{for } x \in S_i \\ \mathbf{a}_y \equiv (\langle y \rangle, \langle y - x \rangle) & \text{for } y \in S_i \end{cases} \quad (8)$$

Here x and y denote respectively CMOD5 and CMOD5.N wind speed, S_i are pre-defined speed bins of $2.5 m s^{-1}$ and given WVC and $\langle \cdot \rangle$ set-wise averages. Only subsets with 100 winds or more are plotted. The averaging is necessary to disentangle (pseudo) biases introduced by the discretization of wind speed bins into $0.5 m s^{-1}$, which is not small compared to the objective speed difference of $0.7 m s^{-1}$ and affects results at low and high wind speed. A discussion on the usage of weighted bin averages may be found in Section 3.1 of Hersbach *et al.* 2007.

For ASCAT, the results displayed in Figure 8 are based on the inclusion of correction in backscatter, but excluding the post-inversion correction in wind speed. These latter corrections are determined per wind speed bin. Therefore, when CMOD5.N and CMOD5 winds fall in different bins, different (non interpolated) corrections are applied, which would clutter the real difference between the two model functions.

As function of wind speed (top panels of Figure 8) results are similar for ERS-2 and ASCAT. For light winds, wind correction is a few $cm s^{-1}$ less, especially for ERS-2. Correction is maximal for winds around $5 m s^{-1}$, then decreases slightly, and for winds above $15 m s^{-1}$ increases again. These variations, which are all within a few $cm s^{-1}$, are in agreement with what was anticipated during the CMOD5.N fit, and are reflected in the right panel of Figure 4. As function of wave vector cell (lower panels of Figure 8) variation is small for ASCAT, while for ERS-2 winds are slightly more enhanced at low WVC.

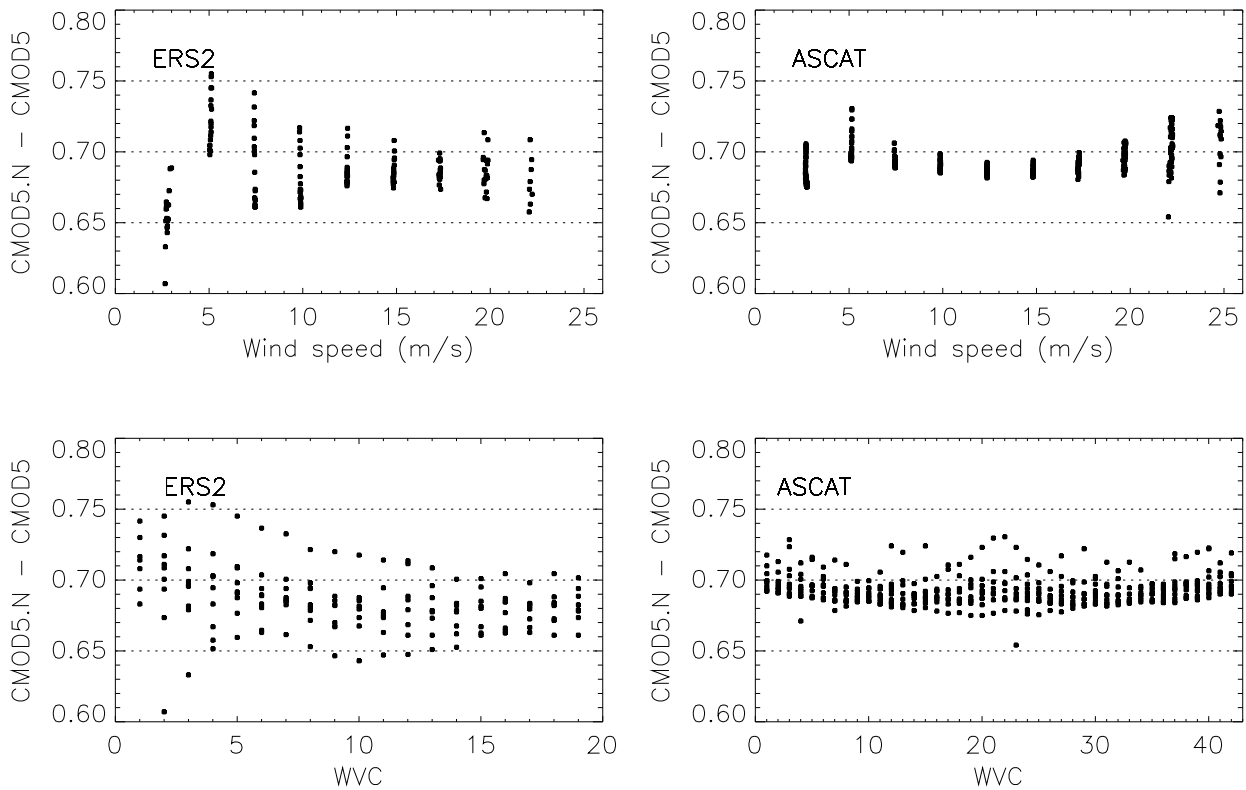


Figure 8: Difference between CMOD5.N and CMOD5 wind speed after inversion of respectively ERS-2 backscatter triplets (left), and ASCAT triplets (right) accumulated over July 2007 and January 2008. Data points represent WVC-wise and speed bin-wise (of 2.5m s^{-1}) averages for which at least 100 data points were available, and are displayed as function of respectively wind speed (top panels), and WVC (lower panels).

Differences in wind direction between CMOD5.N and CMOD5 appear small. Scatter diagrams for ERS-2 and ASCAT data are presented in respectively the left-hand and right-hand panel of Figure 9. The low relative standard deviation of respectively 4.2 and 3.3 degrees, are again, mainly the result of discretization. At specific α angles, there are some differences. The fact that these occur at 45 degree intervals, indicates that they probably arise from cases where the determination of wind direction was troublesome for the PRESCAT algorithm to start with.

5 The effect of stability on scatterometer departures

For the two periods, July 2007 and January 2008, ERS-2 and ASCAT winds based on CMOD5.N are collocated with ECMWF neutral winds, using the setup as described in the last part of Section 2. Short-range forecast winds are used rather than analysis winds, to minimize the effect of correlation with the operationally assimilated ERS-2 and ASCAT product. Summed over both periods, the entire globe and all WVCs, the comparison is good, as can be seen in Figure 10. For ERS-2 the overall bias is small (-0.03 m s^{-1}). Although ASCAT winds are somewhat lower (bias of -0.11 m s^{-1}), one should realize that the corrections in backscatter and wind speed domain, as described above, had for ASCAT not been carefully tuned to buoy data. In addition, the difference in coverage between ERS-2 (non-global) and ASCAT (global) may induce differences in statistics. As function of WVC, bias varies between -0.26 m s^{-1} and 0.10 m s^{-1} for ERS-2 and between -0.19 m s^{-1} and -0.04 m s^{-1} for ASCAT. A more detailed view is presented in Figure 11. Each point represents the average

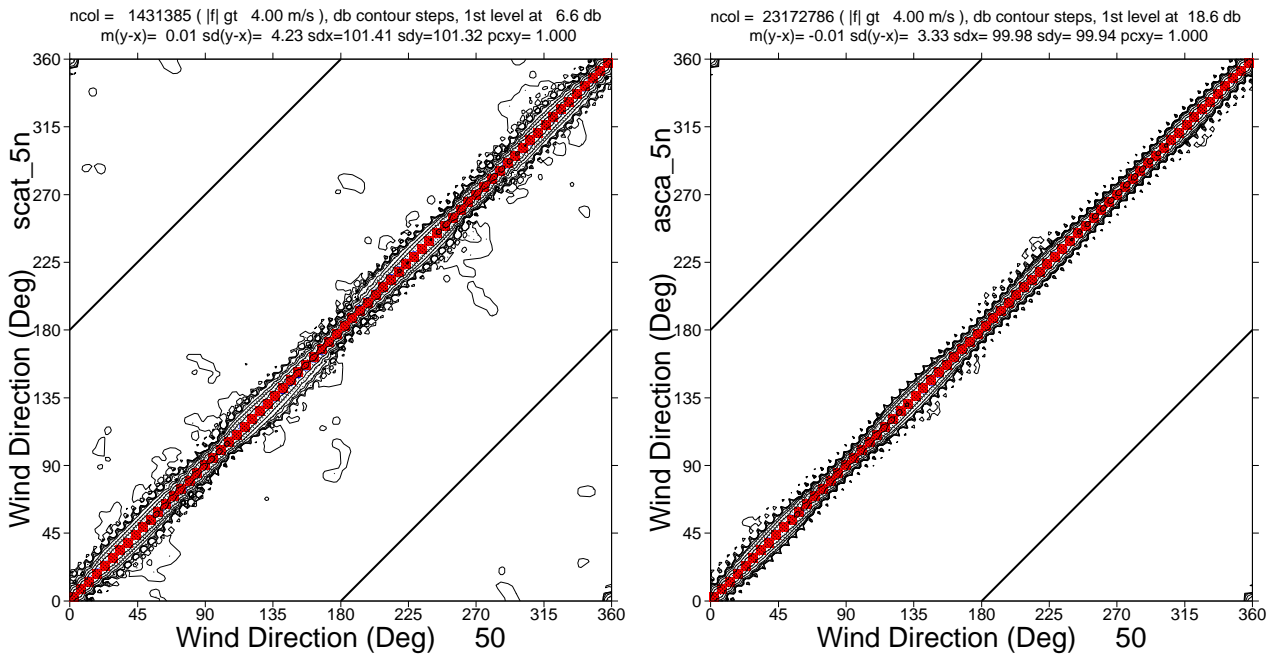


Figure 9: Same inversion as in Figure 8, but now for wind direction and limited to cases in which both CMOD5.N and CMOD5 wind speed are at least 4 m s^{-1} , and represented as a scatter diagram. Contours are in steps of 5 dB. Blue circles denote averages for bins in the x-direction, and red squares averages for bins in the y-direction.

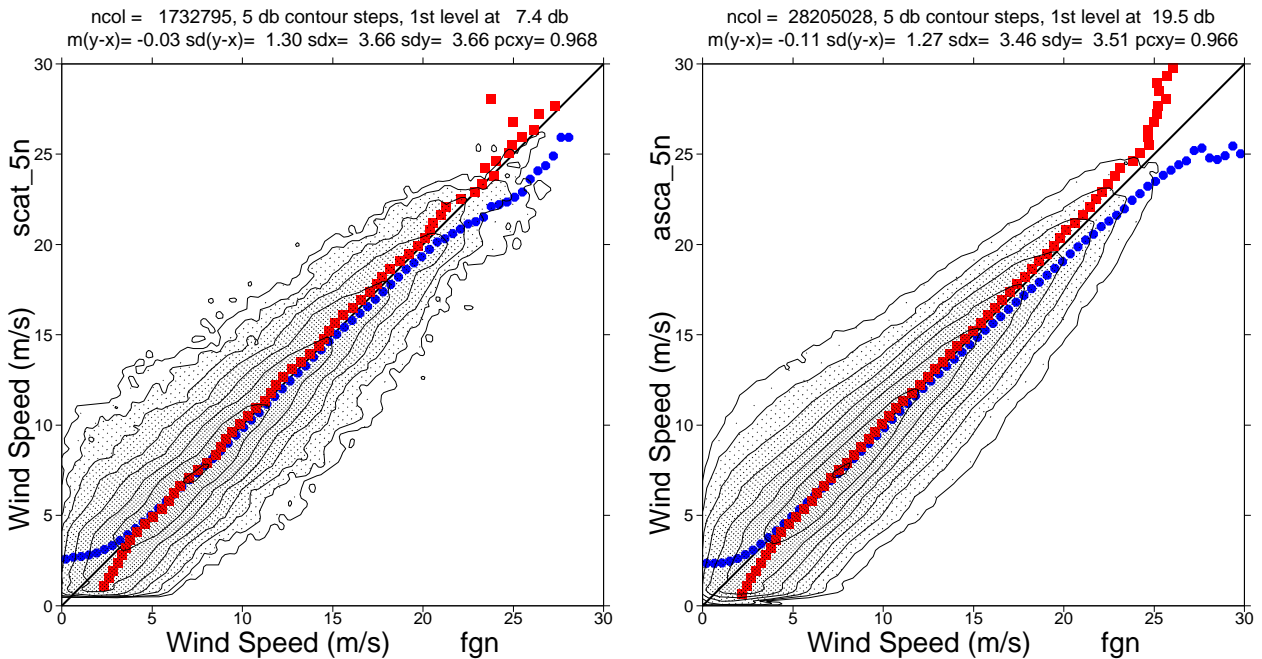


Figure 10: Same inversion as in Figure 8, but now for the difference between CMOD5.N wind and collocated ECMWF equivalent short-range forecast wind at 10m. Contours are in steps of 5 dB. Blue circles denote averages for bins in the x-direction, and red squares averages for bins in the y-direction.

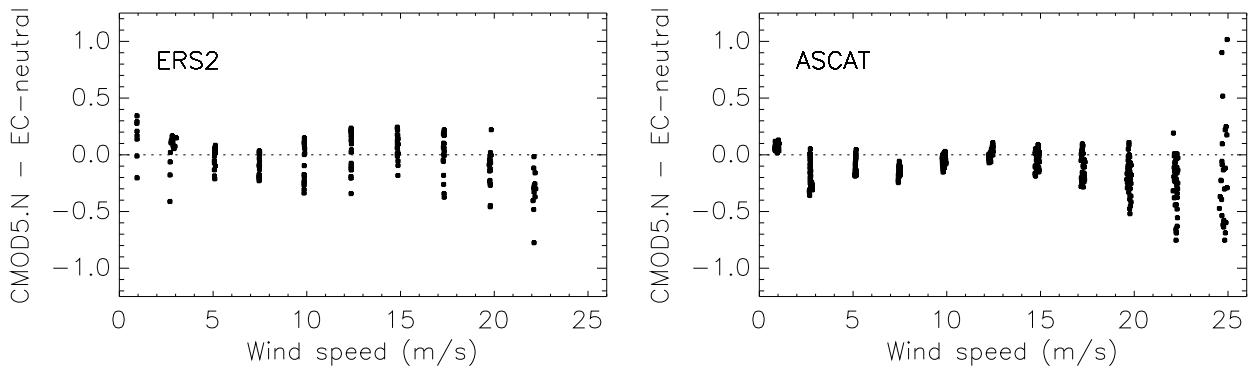


Figure 11: Same as for Figure 3 and top panels of Figure 8, but now for CMOD5.N wind speed versus collocated ECMWF neutral wind.

as defined in Eq.(8) for a set (of at least 100 data points) restricted to a specific WVC and certain speed bin (width of 2.5m s^{-1}). From this it is seen that variations as function of wind speed and WVC are mild. Only for extreme winds, ERS-2 wind speed is somewhat lower, while for ASCAT there are inter-node differences. Statistics here, though, is low.

The relative standard deviation between CMOD5.N and ECMWF neutral winds (1.30m s^{-1} for ERS-2, 1.27m s^{-1} for ASCAT) is slightly lower than the standard deviation with ECMWF non-neutral winds (1.35m s^{-1} for ERS-2, and 1.30m s^{-1} for ASCAT; not shown). This indicates that, indeed, some of the scatter between scatterometer and ECMWF wind can be explained by the effect of stability corrections. To investigate this further, maps of average departures for ASCAT data are presented in Fig. 12. Similar results are obtained for ERS-2 in areas of data coverage (not shown). To undo the effect of the difference between neutral and non-neutral wind of 0.20m s^{-1} , in these maps, global average values have been subtracted. It is seen that at various locations relative bias levels have improved. This is, e.g., the case for the stable areas in summer in the North-American Great Lakes, east of Newfoundland, and large areas along the Antarctic Circumpolar Current. Connected to unstable stratification in winter, relative biases in the Kuroshio Extension and around the Gulf stream have diminished. In the tropics, biases have tempered at various locations as well. In the Equatorial Pacific, for instance, the dipole of positive and negative bias has been slightly reduced. The residue is connected with the presence of the South Equatorial Current and Equatorial Counter Current, and the fact that a scatterometer senses wind (stress) relative to the moving surface (Kelly *et al.* 2001).

Although corrections work in general in the proper direction, the difference between neutral and non-neutral wind only explains part of the average bias between scatterometer and ECMWF model winds. Part of the remainder could be due to stability-dependent errors in the ECMWF boundary layer formulation. As, e.g., pointed out by Brown *et al.* (2006), in the ECMWF model formulation (as well as in The Met Office model), momentum mixing seems too strong in the stable boundary layer and too weak under unstable conditions. Within this study a triple collocation study between ECMWF, QuikSCAT, and winds from a number of buoys platforms from the U.S. National Data Buoy Center (NDBC), indicated that the relative bias between scatterometer and buoy wind did not show a clear dependence on stability. As a consequence, neutral ECMWF winds under stable conditions are thought to be too strong, under unstable conditions too weak, and this shows up as a residual bias when compared to neutral scatterometer winds.

As is seen from Fig. 12, there are also several areas in which the local biases between scatterometer and model wind do not seem to be connected with stability. Examples are orographic effects (Xie *et al.* 2001, Chelton *et al.* 2004) and current effects (Kelly *et al.* , 2001). Scatterometer winds seem consistently stronger in the

vicinity of land and sea ice. One explanation is a lack in the land-sea gradient in ECMWF wind speed due to the limited horizontal resolution (25km). Near the poles, contamination of scatterometer data by ice would lead to erroneously high winds. However, the screening used at ECMWF, at which the data used in Fig. 12 are also subjected, is rather conservative (Hersbach and Janssen, 2007), and should take care of most of ice problems. Another reason for biases near land and ice could be given by sea-state dependencies. Near coastal areas with on average off-land wind conditions, ocean surface waves are younger and steeper, with on average an enhanced surface roughness z_0 (see e.g., Janssen, 1991). Given a certain value of (neutral) wind speed at 10-metre height z , the underlying surface stress has to be larger when z_0 is larger, since the drag coefficient C_D scales as $C_D \sim 1/\log(z/z_0)^2$. Such enhanced stress will lead to an enhanced scatterometer wind, since that transformation has been trained on a global average, lower, roughness length. Maps of average values of ECMWF surface roughness (not shown) display an enhanced roughness near ice edges in the winter Arctic and Antarctic. This coincides with the larger positive scatterometer bias in these areas compared to the situation in summer. In the eastern part of the North Atlantic off-land wind conditions enhance surface roughness in winter, while roughness is average during summer, when southerly maritime winds are more common. Again, this matches qualitatively with the biases as displayed in the lower panels of Figure 12. A discussion on sea-state effects on C-band scatterometer data can be found in Quilfen *et al.* (2004).

In the Gulf of Guinea large differences exist. Here ECMWF model winds consistently seems to underestimate wind speed by 1 to 2 m s^{-1} , where wind speed is in general low to start with ($\sim 4 \text{ m s}^{-1}$). Long-term monitoring of scatterometer data at ECMWF shows that these biases exist at least since the availability of ERS1 data in 1992. The alleged under estimation of model wind speed is confirmed by wind data from the Soul Pirata buoy at ($0^\circ 0 \text{ N}, 0^\circ 0 \text{ E}$) (Bidlot 2008, private communication). A more detailed view on this bias shows that the model winds lack convergence in the inter-tropical convergence zone (ITCZ) in this region. Between May and August the negative bias usually appears milder, for the simple reason that the ITCZ is then located more over West Africa. During that period, a shift of the ITCZ in the ECMWF model appears responsible for incorrect precipitation forecasts in the region studied by the African Monsoon Multidisciplinary Analyses project (AMMA, see e.g., Agusti-Panareda and Beljaars, 2008).

Sofar attention has been focused on the average departure between scatterometer and model wind. In addition to a reduction of local biases, the random error between scatterometer and model wind appears smallest for neutral winds as well. This can be seen as the result of a positive local correlation between scatterometer departures and stability corrections on shorter (synoptic) time scales. Let d_n and d denote the departure of CMOD5.N wind from respectively ECMWF neutral and non-neutral wind speed, and η the correction in stability:

$$\left. \begin{aligned} d_n &= \text{CMOD5.N} && - && \text{ECMWF neutral} \\ d &= \text{CMOD5.N} && - && \text{ECMWF non-neutral} \\ \eta &= \text{ECMWF neutral} && - && \text{ECMWF non-neutral} \end{aligned} \right\} \implies d_n = d - \eta. \quad (9)$$

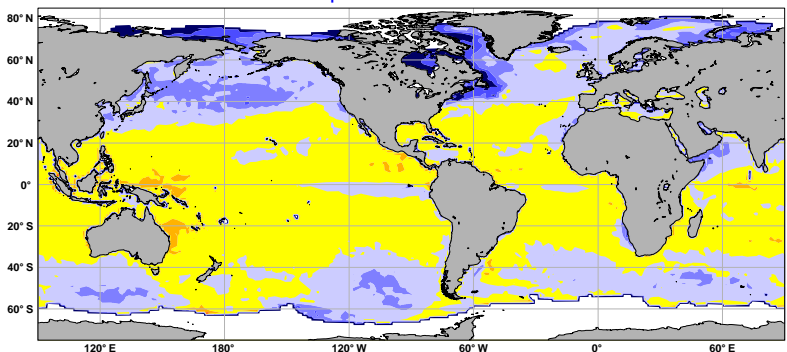
The correlation C between departures and stability corrections can be expressed as:

$$C(d, \eta) = ([\sigma_d^2 - \sigma_{d_n}^2] + \sigma_\eta^2) / (\sigma_d \sigma_\eta) \quad (10)$$

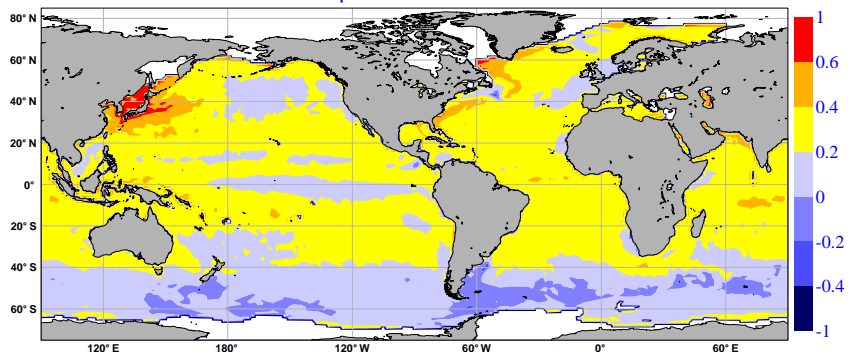
$$C(d_n, \eta) = ([\sigma_d^2 - \sigma_{d_n}^2] - \sigma_\eta^2) / (\sigma_{d_n} \sigma_\eta) \quad (11)$$

where $\sigma_x^2 = \langle (x - \langle x \rangle)^2 \rangle$, $C(x, y) = (\langle xy \rangle - \langle x \rangle \langle y \rangle) / (\sigma_x \sigma_y)$ are the usual definitions, and $\langle . \rangle$ denotes location-wise averages. The fact that for most areas σ_{d_n} appears slightly lower than σ_d means that $C(d, \eta)$ must be positive. Maps for location-wise correlations are displayed in Figure 13. Indeed, the correlation between non-neutral departure and stability correction is positive almost everywhere, with values that locally can exceed 0.6. Largest correlation is typically found in areas where the fluctuations in stability are largest (top panels of Figure 13). The correlation for neutral departures is much lower. For July 2007, the global average does not show a correlation anymore. Locally some positive and negative correlations remain. For January

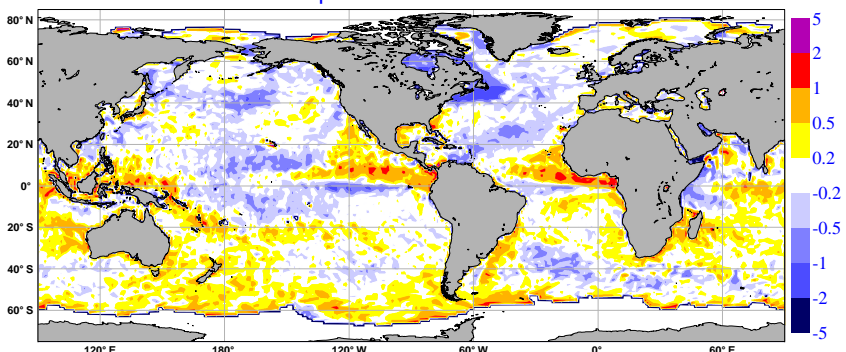
Speed bias of neutral vs non-neutral ECMWF 10-metre wind (m/s), 200707
 Globe 0.2 N.Hem 0.1 Tropics 0.27 S.Hem 0.19 MIN -1.12 MAX 0.5



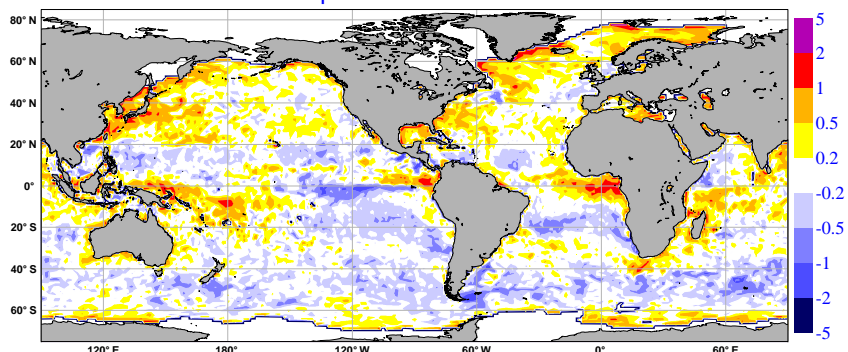
Speed bias of neutral vs non-neutral ECMWF 10-metre wind (m/s), 200801
 Globe 0.22 N.Hem 0.29 Tropics 0.27 S.Hem 0.14 MIN -0.33 MAX 0.72



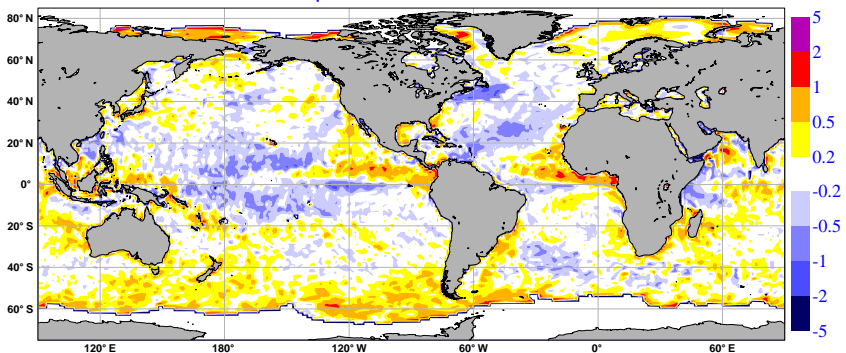
Anomaly of wind speed bias (ASCAT vs non-neutral) in m/s, 200707
 Globe 0 N.Hem -0.17 Tropics 0.02 S.Hem 0.11 MIN -3.73 MAX 8.55



Anomaly of wind speed bias (ASCAT vs non-neutral) in m/s, 200801
 Globe 0 N.Hem 0.2 Tropics 0 S.Hem -0.11 MIN -1.92 MAX 2.69



Anomaly of wind speed bias (ASCAT vs neutral) in m/s, 200707
 Globe 0 N.Hem -0.07 Tropics -0.05 S.Hem 0.11 MIN -3.33 MAX 8.75



Anomaly of wind speed bias (ASCAT vs neutral) in m/s, 200801
 Globe 0 N.Hem 0.14 Tropics -0.04 S.Hem -0.03 MIN -1.83 MAX 2.64

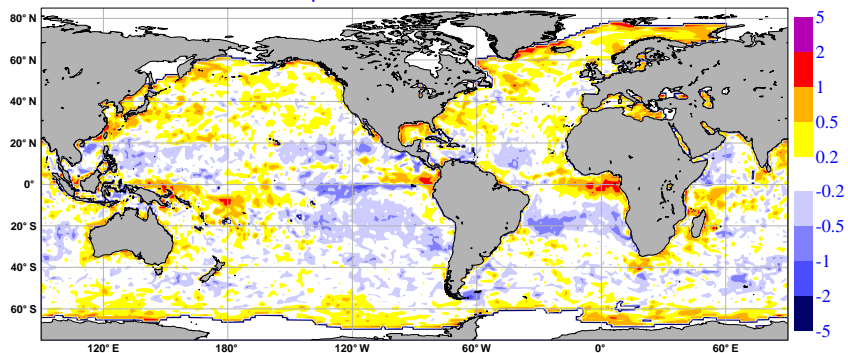


Figure 12: Average difference between ECMWF neutral and non-neutral wind speed (top panels), and anomaly from the global mean of ASCAT departures from ECMWF non-neutral (middle panels) and neutral (lower panels) wind accumulated over respectively July 2007 (left panels) and January 2008 (right panels), and gridded into boxes on a N80 reduced Gaussian grid (average box size is 1.125 by 1.125 degrees). Winds are based on CMOD5.N, and the global mean departures are respectively 0.09 m s^{-1} (non-neutral) and -0.11 m s^{-1} (neutral). Note a difference in color scaling between the top and the other panels.

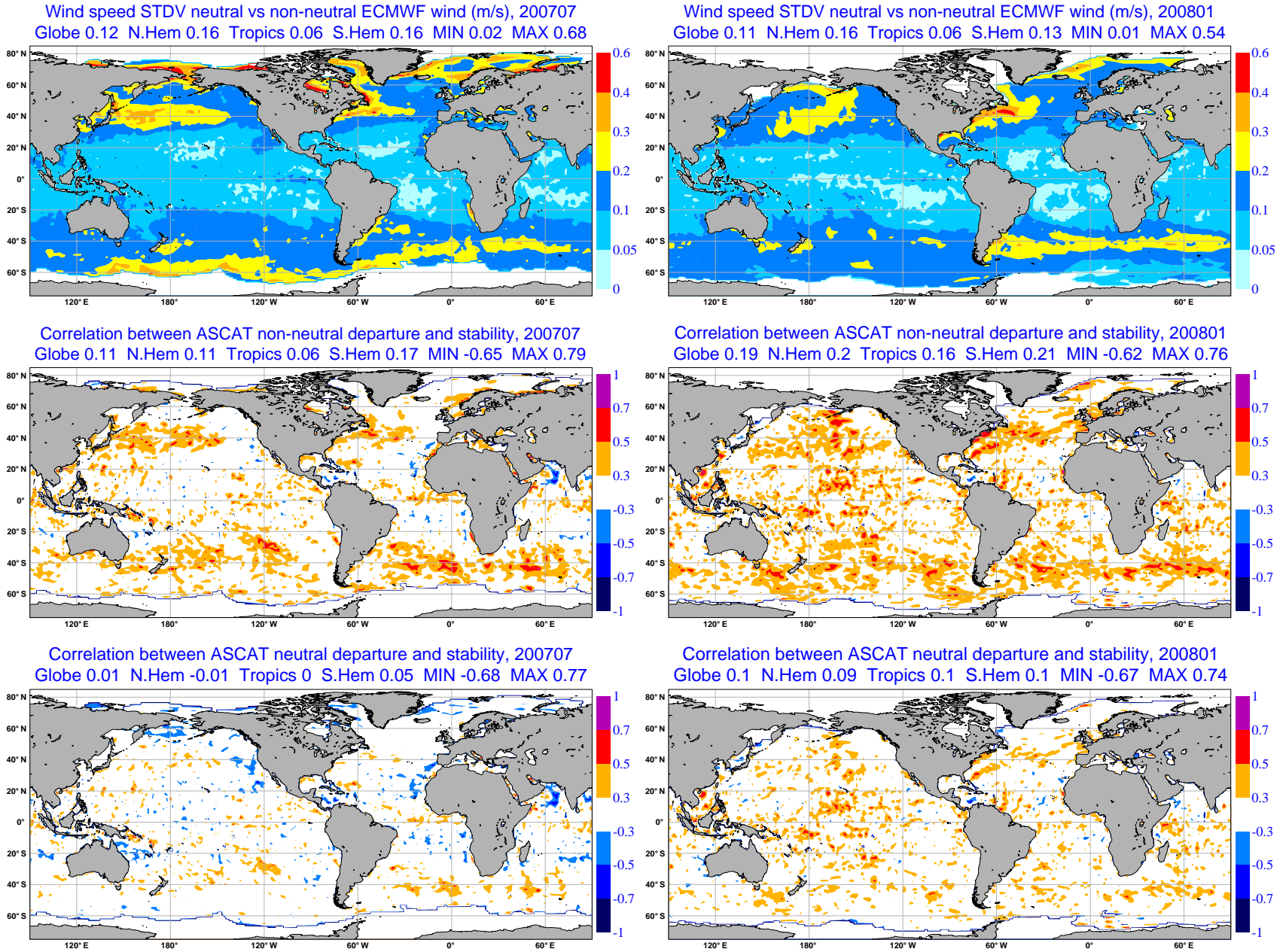


Figure 13: Standard deviation of local fluctuations in stability corrections (top panels), and the correlation with ASCAT wind speed departures (middle panels non-neutral; lower panels neutral) for subsets collected per N80 reduced Gaussian grid box and accumulated over respectively July 2007 (left panels) and January 2008 (right panels).

2008, there is still a residual global positive correlation (0.10). Non-neutral correlation (of 0.19) is for this month also larger than for July 2007 (0.11).

6 Concluding remarks

The initial experience with the CMOD5.N geophysical model function is promising. Besides providing a model function that relates to neutral wind rather than non-neutral wind, CMOD5.N resolves a reported bias in the literature of 0.5 ms^{-1} for CMOD5 when compared to buoy data.

For ERS-2 and ASCAT winds inverted on the basis of CMOD5.N compare on average well with ECMWF short-range neutral forecast wind. As expected, the agreement is better than that with non-neutral model wind. Locally, average, seasonally dependent departures are tempered in many areas around the globe, and the relative local standard deviation is slightly reduced. The mostly positive local correlation between scatterometer departures from model wind and corrections for atmospheric stability, has reduced. These findings indeed indicate that part of the difference between scatterometer wind and non-neutral model wind are related to stability. However, a residual stability-dependent difference between scatterometer and neutral model wind remains. This difference is consistent with the observation by Brown *et al.* (2006), that in the ECMWF boundary layer formalism, momentum mixing seems too strong under stable and too weak under unstable conditions.

Besides residual stability-dependent differences, effects by orography and ocean currents are clearly visible. In addition, the relative scatterometer bias seems related to sea-state effects, such as variations in the surface roughness length due to the local ocean surface wave age. This confirms that a scatterometer is sensitive to surface stress. Although the concept of equivalent-neutral wind is able to incorporate the effect of atmospheric stability on surface wind, it does not do so for sea-state effects, and only an appropriate geophysical model function for stress could account for these.

Acknowledgements

The author would like to thank Peter Janssen, Ad Stoffelen, Jean Bidlot, Peter Bechtold, Martin Köhler, Anna Agusti-Panareda and Martin Miller for their useful discussions and suggestions.

References

- Abdalla S. and Hersbach H. (2007). The technical support for global validation of ERS Wind and Wave Products at ECMWF (April 2004 - June 2007), *Final report for ESA contract 18212/04/I-LG, ECMWF, Shinfield Park, Reading*.
http://www.ecmwf.int/publications/library/ecpublications/_pdf/esa/ESA_abdalla_hersbach_182122007.pdf
- Agusti-Panareda, A., Beljaars, A. (2008). ECMWF's contribution to AMMA, *ECMWF Newsletter* **115**.
- Attema, E., P., W. (1986). An experimental campaign for the determination of the radar signature of the ocean at C-band, *Proc. Third International Colloquium on Spectral Signatures of Objects in Remote Sensing*, Les Arcs, France, ESA, SP-247, 791-799, 1986.
- Brown, A. R., Beljaars, A. C. M., Hersbach, H. (2006). Errors in parametrizations of convective boundary layer turbulent momentum mixing *Quart. J. Roy. Meteor. Soc.* **132**, 1,859-1,876

- Carswell, J. R., W. J. Donnelly, R. E. McIntosh, M. A. Donelan, and D. C. Vandemark (1999a), Analysis of C and Ku band ocean backscatter measurements under low-wind conditions, *J. Geophys. Res.*, **104** (C9), 20,687-20,701.
- Chelton, D. B., Schlax, M. G., Freilich, M. H., and R. F. Milliff (2004) Satellite Measurements Reveal Persistent Small-Scale Features in Ocean Winds, *Science.*, **303**, 978-983.
- Chelton, D. B., and M. H. Freilich (2005) Scatterometer-Based Assessment of 10-m Wind Analyses from the Operational ECMWF and NCEP Numerical Weather Prediction Models, *Mon. Wea. Rev.*, **133**, 409-429.
- Donnelly, W. J., J. R. Carswell, R. E. McIntosh, P. S. Chang, J. Wilkerson, F. Marks, and P. G. Black (1999), Revised Ocean Backscatter Models at C and Ku-band under High-wind Conditions, *J. Geophys. Res.*, **104** (C5), 11,485-11,497.
- Esteban, F. D., J. R. Carswell, S. Frasier, P. S. Chang, P. G. Black, and F. D. Marks (2006) Dual-polarized C- and Ku-band ocean backscatter response to hurricane-force winds *J. Geophys. Res.*, **111** (C8).
- J. Figa-Saldaña, J.J.W. Wilson, E. Attema, R. Gelsthorpe, M.R. Drinkwater, and A. Stoffelen, 2002. The advanced scatterometer (ASCAT) on the meteorological operational (MetOp) platform: A follow on for European wind scatterometers. *Can. J. Remote Sensing*, **28**, 404-412.
- Francis, R., G. Graf, P. G. Edwards, M. McCaig, C. McCarthy, P. Dubock, A. Lefebvre, B. Pieper, P. Y. Pouvreau, R. Wall, F. Wechsler, J. Louet, and R. Zobl (1991) The ERS-1 spacecraft and its payload. *ESA Bulletin*, (65):27-48, Feb. 1991. ERS-1 Special Issue.
- Freilich, M. H., and Dunbar R. S. (1999). The accuracy of the NSCAT 1 vector winds: comparisons with National Data Buoy Center buoys, *J. Geophys. Res.*, **104** (C5), 11,231-11,246.
- Ebuchi, N, H. C. Graber, and M. J. Caruso (2002), Evaluation of Wind Vectors Observed by QuikSCAT/SeaWinds Using Ocean Buoy Data, *J. Atmos. Ocean. Technol.*, **19**, 2,049-2,062.
- Hersbach H., Stoffelen A., and Haan de S., 2007, An improved C-band scatterometer ocean geophysical model function: CMOD5, *J. Geophys. Res.*, **112** (C3) C03006.
- H. Hersbach and P. Janssen, 2007. Improved scatterometer screening. *ECMWF Research Department Memorandum R60.9/HH/0735*
- IFS documentation, (2004). edited by P. White, <http://www.ecmwf.int/research/ifsdocs/CY28r1/>
- Isaksen, L., and Janssen P. A. E. M. (2004). The benefit of ERS Scatterometer Winds in ECMWF's variational assimilation system. *Q. J. R. Meteorol. Soc.* **130** 1793-1814,
- Janssen P. A. E. M. (1991). Quasi-linear theory of wind wave generation applied to wave forecasting. *J. Phys. Oceanogr.* **21** 1631-1642.
- Kelly, A. K., Dickinson, S., McPhaden, J., and G. C. Johnson (2001). Ocean Currents Evident in Satellite Wind Data. *Geoph. Res. Lett.* **28** 2469-2472.
- Long, A. E. (1984). Towards a C-Band radar sea echo model for the ERS-1 scatterometer, *Proc. Third International Colloquium on Spectral Signatures of Objects in Remote Sensing*, Les Arcs, France, ESA, SP-247, 29-34.
- Offiler, D (1994), The Calibration of ERS-1 Satellite Scatterometer Winds, *J. Atmos. Oceanic Technol.*, **11**, 1,002-1,017.

Portabella M., and Stoffelen A., 2007. Development of a global Scatterometer Validation and Monitoring, to appear at: <http://www.knmi.nl/publications/>

Quilfen, Y., B. Chapron, F. Collard, and D. Vandemark (2004) Relationship between ERS Scatterometer Measurement and Integrated Wind and Wave Parameters, *J. Atmos. Oceanic Technol.*, **21**, 368-373.

Stoffelen, A. C. M., and Anderson D. L. T. (1997). Scatterometer Data Interpretation: Derivation of the Transfer Function CMOD4, *J. Geophys. Res.*, **102** (C3) 5,767-5,780.

A. Stoffelen, 1999. A simple method for calibration of a scatterometer over the ocean. *J. Atmos. Oceanic Technol.*, **16**, 275-282.

J. Verspeek, M. Portabella, A. Stoffelen and A. Verhoef, 2007. Calibration and Validation of ASCAT Winds, version 2.1 Document external project: 2007, SAF/OSI/KNMI/TEC/TN/163, EUMETSAT, available at: <http://www.knmi.nl/scatterometer/publications/>

Wentz, F. J., and D. K. Smith (1999) A model function for the ocean-normalized radar cross section at 14 GHz derived from NSCAT observations, *J. Geophys. Res.*, **104** (C5) 11,499-11,514.

Xie, S. P., Liu, W. T., Qinyu Liu, Nonaka, M., and Hafner, J (2001) Long-range effects of the Hawaiian Islands on the Pacific-Ocean-atmosphere system. *Geoscience and Remote Sensing Symposium, 2001. IGARSS apos 01. IEEE 2001 International* **3** 1086-1088